Tailoring Longitudinal Surface Plasmon Wavelengths, Scattering and Absorption Cross Sections of Gold Nanorods

Weihai Ni, Xiaoshan Kou, Zhi Yang, and Jianfang Wang*

Department of Physics, The Chinese University of Hong Kong, Shatin, Hong Kong SAR, P. R. China

ABSTRACT Tailoring the longitudinal surface plasmon wavelengths (LSPWs), scattering, and absorption cross sections of gold nanorods has been demonstrated by combining anisotropic shortening and transverse overgrowth and judiciously choosing starting Au nanorods. Shortening yields Au nanorods with decreasing lengths but a fixed diameter, while overgrowth produces nanorods with increasing diameters but a nearly unchanged length. Two series of Au nanorods with LSPWs varying in the same spectral range but distinct extinction coefficients are thus obtained. The systematic changes in the LSPW and extinction for the two series of Au nanorods are found to be in good agreement with those obtained from Gans theory. Dark-field imaging performed on two representative nanorod samples with similar LSPWs shows that the scattering intensities of the overgrown nanorods are much larger than those of the shortened nanorods. The experimental results are found to be in very good agreement with those obtained from finite-difference time-domain (FDTD) calculations. FDTD calculations further reveal that the scattering-to-extinction ratio increases linearly as a function of the diameter for Au nanorods with a fixed aspect ratio.

KEYWORDS: gold nanorods · surface plasmon resonance · absorption · scattering · extinction · dark-field imaging

Gold nanorods exhibit transverse and longitudinal surface plasmon resonances that correspond to electron oscillations perpendicular and parallel to the rod length direction, respectively. Their longitudinal surface plasmon wavelengths (LSPWs) are tunable from the visible to infrared regions. Their absorption cross sections are at least five orders larger than those of conventional dyes, and the light scattering by Au nanorods is several orders larger than the light emission from strongly fluorescent dyes.[1–3] The tunability in the LSPW, together with strongly enhanced scattering and absorption at the LSPW, makes Au nanorods useful for the formation of many functional composite materials, for example, with hydrogel,[4,5] polymers,[6,7] silica,[8] and bacteria.[9] Au nanorods also offer advantages of good biocompatibility, facile preparation, and conjugation with a variety of biomolecular ligands, antibodies, and other targeting moieties.[10] They have therefore found wide applications in biochemical sensing,[11] biological imaging, medical diagnostics, and therapeutics.[12–16]

The effectiveness of Au nanorods as scattering-based biomedical imaging contrast agents and as photothermal therapeutic agents is strongly dependent on their scattering and absorption cross sections. In general, high scattering cross sections are favorable for cellular and biological imaging based on dark-field microscopy, while large absorption cross sections with small scattering losses allow for photothermal therapy with a minimal laser dosage. In addition, the LSPWs of Au nanorods are strongly desired to be in the spectral range of 650–900 nm. Light irradiation in this region can penetrate deeper in tissues and cause less photodamage than UV–visible irradiation.[17] Therefore, the ability to tailor both scattering and absorption of Au nanorods with different LSPWs is of ultimate importance for practical *in vivo* biomedical imaging and therapeutic applications.[18–20] Although the control of the LSPWs of Au nanorods has been demonstrated in a large number of experiments,[21–28] the experimental ability to specifically tailor their scattering and absorption cross sections has remained elusive.

We have recently demonstrated anisotropic shortening[29] and transverse overgrowth[30] of Au nanorods. Here we demonstrate the tailoring of the scattering and absorption cross sections of Au nanorods by combining anisotropic shortening and transverse overgrowth together and using the same batch of starting Au nanorods. Shortening produces thin nanorods, while overgrowth yields fat nanorods. The changes in the LSPW and extinction coefficient extracted from the extinction spectra

See the accompanying Perspective by Odom and Nehl on p 612.

*Address correspondence to jfwang@phy.cuhk.edu.hk.

Received for review November 10, 2007 and accepted March 04, 2008.

Published online March 20, 2008.
10.1021/nn7003603 CCC: $40.75

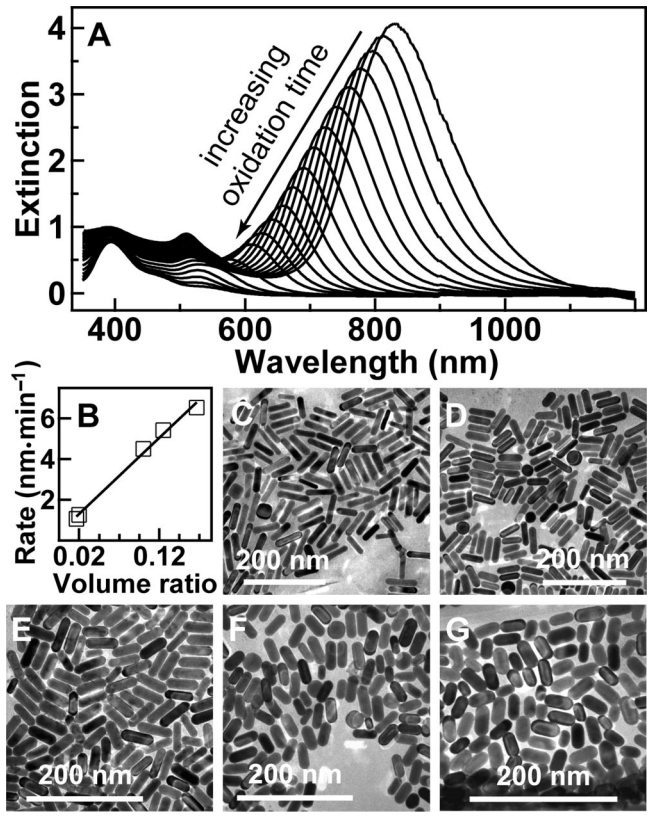

Figure 1. Shortening of Au nanorods. (A) Extinction spectra acquired every 2.5 min after the addition of H_2O_2. The volume ratio of H_2O_2 to the starting nanorod solution is 1:6. The extinction curves have been scaled relative to the starting nanorod concentration. (B) Nanorod shortening rate versus the volume ratio between H_2O_2 and the nanorod solution. The line is a linear fit. (C)−(G) TEM images of representative Au nanorod samples obtained at varying stages of oxidation. The volume ratio between H_2O_2 and the nanorod solution is 1:60. The oxidation time is 2, 3, 3.7, 5, and 5.5 h for (C)−(G), respectively.

of the two series of nanorod samples are found to be in good agreement with those obtained from the modeling based on Gans theory. Single-particle dark-field imaging and spectroscopy performed on two representative batches of nanorod samples with similar LSPWs show that the scattering intensities of the overgrown nanorods are more than 1 order of magnitude larger than those of the shortened nanorods. The experimentally measured scattering intensity ratio between the two batches of nanorod samples is close to that obtained from finite-difference time-domain (FDTD) calculations. FDTD calculations further show that for Au nanorods with a fixed aspect ratio the scattering-to-absorption ratio increases as the diameter is increased. Absorption is dominant for thin nanorods, while scattering becomes dominant for fat nanorods.

RESULTS AND DISCUSSION

Shortening and Overgrowth. Anisotropic shortening and transverse overgrowth are carried out using the same batch of starting Au nanorods. Because the total number of nanorods remains unchanged throughout the shortening and overgrowth process, the extinction cross sections of the resulting two series of Au nanorods can be quantitatively compared by acquiring their ensemble extinction spectra. A typical transmission electron microscopy (TEM) image of the starting nanorods is shown in Figure S1A in the Supporting Information. Their sizes are relatively uniform, with an average diameter of (17 ± 2) nm, an average length of (74 ± 6) nm, and an average aspect ratio of 4.6 ± 0.8. Figure S1B in the Supporting Information shows the ensemble extinction spectrum. Their longitudinal surface plasmon resonance peak is at 864 nm, with a full width at half-maximum (fwhm) of 190 nm (320 meV). The extinction ratio of the longitudinal surface plasmon resonance peak to the transverse one reaches 5.0, suggesting that the percentage of nanorods in the solution is extremely high.

The starting Au nanorods were shortened through an oxidation reaction. H_2O_2 was used as the oxidizing agent because it is easy to handle and heating is not required, while in our previous shortening experiment, O_2 was used and heating was necessary for the oxidation to occur.[29] Figure 1A shows a sequence of extinction spectra taken as a function of the reaction time right after the addition of H_2O_2. The longitudinal surface plasmon resonance peak blue-shifts gradually and decreases in intensity during oxidation. It then becomes a shoulder of the transverse surface plasmon resonance peak and merges together with the latter. The merging of the two plasmon peaks suggests the transformation of nanorods into nanospheres. Au nanospheres are eventually completely oxidized, as indicated by the final disappearance of the single extinction peak. In addition, a weak peak appears around 400 nm, which results from the metal–ligand charge transfer absorption of $AuBr_4^-$, suggesting the oxidation of Au(0) to Au(III) by H_2O_2. In comparison, Au(0) is oxidized into Au(I) when O_2 is used.[29]

The LSPW changes approximately linearly as a function of the oxidation time. The absolute value of the slope obtained by linearly fitting the curve of the LSPW *versus* the oxidation time can therefore be used to quantify the shortening rate of Au nanorods under different conditions. The shortening rate can be simply controlled by varying the volume ratio between H_2O_2 and the starting nanorod solution, which is another advantage of using H_2O_2 as the oxidant. A plot of the shortening rate (Figure 1B) shows that it increases linearly with the volume ratio between H_2O_2 and the starting nanorod solution.

The oxidation reaction can be stopped at intermediate stages by centrifugation and then redispersion into aqueous solutions if the reaction is sufficiently slow. In this way, Au nanorods with precisely controlled LSPWs can be produced. These nanorods are relatively stable in aqueous solutions, with their LSPWs remaining unchanged for at least one week. Their stability can be further improved by the addition of thiol molecules.[31] Figure 1C−G shows the TEM images of five representative

nanorod samples that were obtained at intermediate stages of oxidation. Clearly, the nanorod length becomes smaller with increasing oxidation time.

Cysteine was used for transverse overgrowth. It carries a thiol group at one end and a carboxyl-amino zwitterionic group at the other end. It can bind selectively to the ends of Au nanorods and thus induce the overgrowth preferentially on the side surfaces of nanorods.[30] The concentration of cysteine in the nanorod solution is important for inducing transverse overgrowth. If it is too high, starting and/or overgrown nanorods will assemble in an end-to-end fashion and precipitate.[32] If it is too low, the overgrowth at the ends of nanorods will not be completely blocked. Figure 2A shows the extinction spectra of the growth products obtained from overgrowth with increasing amounts of the Au precursor. The longitudinal surface plasmon resonance peak blue-shifts, while the transverse one slightly red-shifts as more Au precursor is supplied. Both peaks increase in intensity. Figure 2B−G shows the TEM images of six representative overgrowth products. The nanorods are seen clearly to get fatter as the amount of the Au precursor is increased. They undergo a gradual shape change from rods through peanuts to octahedra. These nanorods are highly stable in aqueous solutions, with their LSPWs remaining unchanged for more than three months. Such a high stability is probably due to their large sizes.

The sizes of the nanorods obtained from shortening and overgrowth were measured from their TEM images. Through the shortening process, the nanorod diameter remains constant, while the nanorod length decreases steadily as a function of the oxidation time (Figure 3A). The plot of the LSPW versus the aspect ratio shows a linear relationship (Figure 3B). A linear fitting of the plot gives a slope of (99 ± 3) nm and an intercept of (412 ± 8) nm. Since the diameter of the nanorods obtained from overgrowth varies along the length direction, the diameter at the middle was measured. Figure 3C shows the variations of the diameter and length *versus* the LSPW. As expected, the diameter increases as the LSPW becomes shorter. In addition, the length also increases when the nanorods are above a certain size, but the increase in the length is slower than that in the diameter. As a result, the aspect ratio gets smaller with increasing amounts of the Au precursor, leading to the blue-shift of the longitudinal plasmon peak. Figure 3D shows the plot of the LSPW versus the aspect ratio of the overgrown nanorods. A linear fitting gives a slope of (94 ± 4) nm and an intercept of (441 ± 12) nm. The slope and intercept obtained for the overgrown nanorods are very close to those obtained for the shortened nanorods, respectively. The observed linear relationship between the LSPW and aspect ratio of Au nanorods is in good agreement with previous experimental results.[21−30]

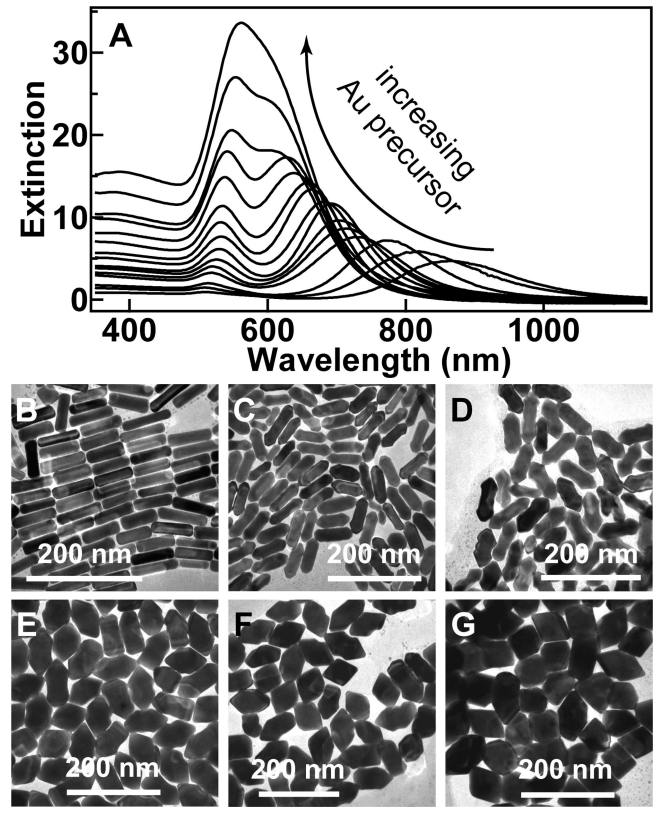

Figure 2. Overgrowth on Au nanorods. (A) Extinction spectra of the growth products obtained by the addition of varying amounts of the Au precursor solution into each aliquot of the starting nanorod solution in the presence of cysteine at appropriate concentrations. The extinction curves have been scaled relative to the starting nanorod concentration. (B)−(G) TEM images of the representative growth products obtained from the overgrowth by the addition of 1, 3, 5, 18, 25, and 30 mL of the Au precursor solution, respectively, into 2 mL of the starting nanorod solution.

The increase in the nanorod length is different from what has been observed in our previous overgrowth experiment, where the nanorod length remains nearly unchanged.[30] The different overgrowth behaviors can be ascribed to the difference in the diameter of the starting nanorods. The diameter of the starting nanorods used in this experiment is (17 ± 2) nm, while that in our previous experiment is (10.3 ± 0.9) nm. The end surface area of the former is 2.7 times that of the latter. The optimal cysteine concentration for a complete blocking of the longitudinal overgrowth is found to be ~0.1 mM in our previous experiment. Because the nanorod concentrations in both experiments are estimated from previously measured extinction coefficients[33,34] to be ~1 nM, it is expected that the optimal cysteine concentration for the fatter starting nanorods used in this experiment should be ~0.27 mM. However, it is found that cysteine at such a concentration causes the precipitation of overgrown nanorods due to cysteine-induced nanorod end-to-end assembly. We therefore used a smaller cysteine concentration, 0.15 mM, for the overgrowth using a small amount of the Au precursor and raised the cysteine concentration to 0.25 mM when a large amount of the Au precursor was used. The use of

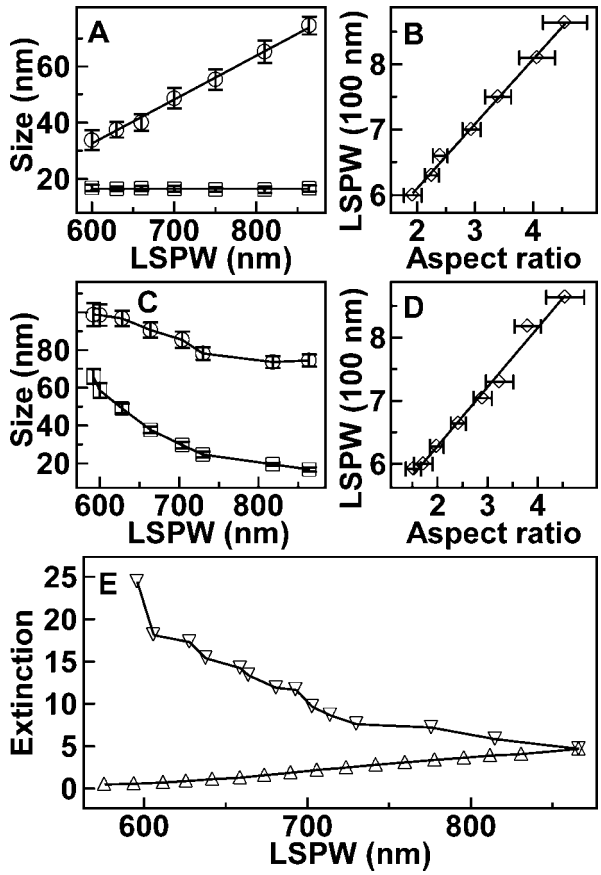

Figure 3. (A) Diameter (squares) and length (circles) changes of the shortened Au nanorods as a function of the LSPW. (B) LSPW *versus* the aspect ratio of the shortened Au nanorods. (C) Diameter (squares) and length (circles) changes of the overgrown Au nanorods as a function of the LSPW. (D) LSPW *versus* the aspect ratio of the overgrown Au nanorods. (E) Peak extinction values extracted from Figure 1A (upper triangles) and Figure 2A (lower triangles) *versus* the LSPWs.

different concentrations of cysteine for the overgrowth of differently sized nanorods leads to an incomplete blocking of longitudinal overgrowth, but can ensure that the overgrown nanorods are well-dispersed without aggregation.

The use of the same starting nanorods for both shortening and overgrowth allows for a quantitative comparison of the extinction values between the two series of resulting Au nanorods. The extinction values extracted from Figures 1A and 2A are plotted together as a function of the LSPW in Figure 3E. They should be proportional to the nanorod extinction cross sections because the total nanorod number remains unchanged throughout both the shortening and overgrowth processes. The extinction values of the shortened nanorods decrease steadily as the LSPW gets smaller, while those of the overgrown nanorods increase with decreasing LSPWs. More importantly, the extinction cross sections of the overgrown nanorods are larger than those of the shortened nanorods. The difference in the extinction cross section between the two series of nanorods gets larger as the LSPW is decreased. This result suggests that we can experimentally tailor the extinction cross sections of Au nanorods with desired LSPWs by judiciously choosing starting nanorods and carrying out anisotropic shortening and transverse overgrowth.

Modeling of the Longitudinal Surface Plasmon Resonance of Gold Nanorods with Gans Theory. Gans theory[35] has been used together with the experimental measured dielectric function for bulk gold[36] to model the extinction spectra of Au nanorods. Previous modeling studies with Gans theory have mainly focused on the dependence of the LSPW on the nanorod aspect ratio and the refractive index of the surrounding medium.[37,38] We use Gans theory to simulate the anisotropic shortening and transverse overgrowth of Au nanorods. In simulation, Au nanorods are treated as prolate spheroids. The major and minor axis lengths are set to 76.8 and 16.7 nm, respectively, which are approximately equal to those of the starting nanorods used in our experiments. For shortening, the nanorod diameter is kept constant, and the nanorod length is reduced step by step. For overgrowth, the nanorod length is kept constant, and the nanorod diameter is increased step by step. Figure 4A shows the modeled extinction spectra. The longitudinal plasmon resonance peak is seen to blue-shift for both shortening and overgrowth. However, the variation in the longitudinal plasmon peak intensity appears different. The intensity decreases gradually for shortening, while for overgrowth, it first increases, reaches a maximum, declines, and then increases again as the aspect ratio is reduced.

The LSPWs and corresponding peak extinction cross sections are extracted from the modeled extinction spectra. The LSPW is found to be independent of the nanorod diameter or length if the aspect ratio is kept fixed (Figure 4B). It increases linearly with the aspect ratio. The slope and the intercept obtained from a linear fitting are (99 $\pm$ 1) nm and (409 $\pm$ 4) nm, respectively. It is interesting to see that the slope and intercept obtained from the modeling are very close to those obtained from both the shortening and overgrowth experiments. Figure 4C shows the variation in the peak extinction cross section as a function of the LSPW. It is clear that the extinction cross sections of the nanorods obtained from overgrowth are generally larger than those from shortening. The overall trends of the two curves look similar to those obtained from the experiments (Figure 3E). For overgrowth, the modeling shows a local extinction maximum around 680 nm, which is not observed on the experimental curve. This can be ascribed to the increase in both the diameter and length of the nanorods obtained from the overgrowth experiment.

Dark-Field Imaging and Spectroscopy. The extinction cross sections of Au nanorods are the sum of the scattering and absorption cross sections. For scattering-based biological imaging, nanorods of large scattering cross sections are desired, while nanorods of high absorption

cross sections benefit absorption-based photothermal therapy. It will therefore be very useful to determine the relative contributions of the scattering and absorption to the extinction of Au nanorods. We used dark-field imaging and spectroscopy to investigate the scattering properties of the nanorods obtained from shortening and overgrowth. This technique has been used previously to study the surface plasmon damping in Au nanorods and the polarization properties of the light scattered from Au nanorods.[39,40] Two nanorod samples that were produced from the same starting nanorods and have similar LSPWs were chosen. One was obtained from shortening, and the other was produced by overgrowth. Their scaled extinction spectra and TEM images are shown in Figure 5. Their average diameters, lengths, and LSPWs are listed in Table 1. The average aspect ratios of both nanorod samples are 2.4 ± 0.3. The maximum extinction value of the longitudinal plasmon peak of the larger nanorods is 8 times that of the smaller nanorods.

The two Au nanorod samples were deposited on silicon and glass substrates for scanning electron microscopy (SEM) and dark-field imaging, respectively. SEM imaging ensures that most nanorods are isolated on substrates without aggregation (Figure 6A−D). The surface number densities determined from SEM images are 50 and 7 per 100 μm^2 for the nanorods obtained from shortening and overgrowth, respectively. Representative dark-field images of the two nanorod samples are shown in Figure 6E and F. The first impression is that the larger nanorods obtained from overgrowth are much brighter in the scattering intensity than the smaller ones obtained from shortening. The scattering intensity histograms (Figure 6G and H) were obtained by measuring the peak intensities of 200–300 nanorods for each sample on the dark-field images. A Gaussian fit was made on both histograms to remove the contributions of aggregated nanorods. The average scattering intensities determined from the Gaussian fit and normalized to the same exposure time are 89 and 3411 counts $\cdot s^{-1}$ for the smaller and larger nanorods, respectively (Table 1). The scattering intensity of the larger nanorods is 38 times that of the smaller ones. The increase in the scattering intensity is much larger than that in the extinction, clearly indicating that the relative contributions of the scattering and absorption to the extinction of Au nanorods with similar LSPWs can be tailored by varying their sizes. In addition, the surface number densities determined from dark-field images are 30 and 8 per 100 μm^2 for the smaller and larger nanorods, respectively, which are roughly consistent with those determined from SEM imaging.

Dark-field scattering spectra of individual nanorods were further recorded by placing a narrow slit at the entrance window of the spectrometer. Representative spectra are shown in Figure 6I and J for the two nanorod samples. The FWHMs of these single-nanorod scattering spectra are about half of those of the ensemble solution extinction spectra (Table 1), indicating that the ensemble extinction spectra are inhomogeneously broadened. In addition, the dark-field scattering spectra are considerably blue-shifted compared to the en-

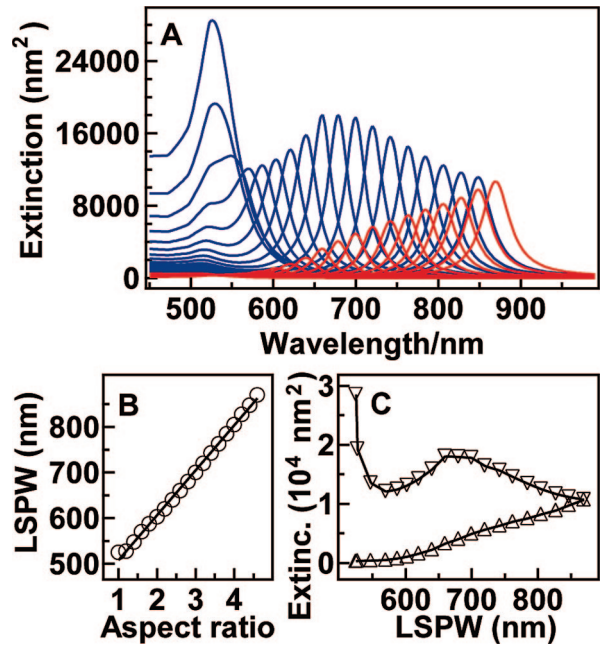

Figure 4. (A) Simulated extinction spectra of Au nanorods. The spectra in red are for anisotropic shortening, where the nanorod diameter is fixed at 16.7 nm and the length is reduced from 76.8 to 16.7 nm from right to left. The spectra in blue are for transverse overgrowth, where the nanorod length is fixed at 76.8 nm and the diameter is increased from 16.7 to 76.8 nm from right to left. The aspect ratio changes from 4.6 to 1.0 at a step of 0.2 for both series of extinction spectra. (B) LSPW changes as a function of the aspect ratio. The line is a linear fit. (C) Peak extinction values *versus* the LSPWs. Upper and lower triangles are for shortening and overgrowth, respectively.

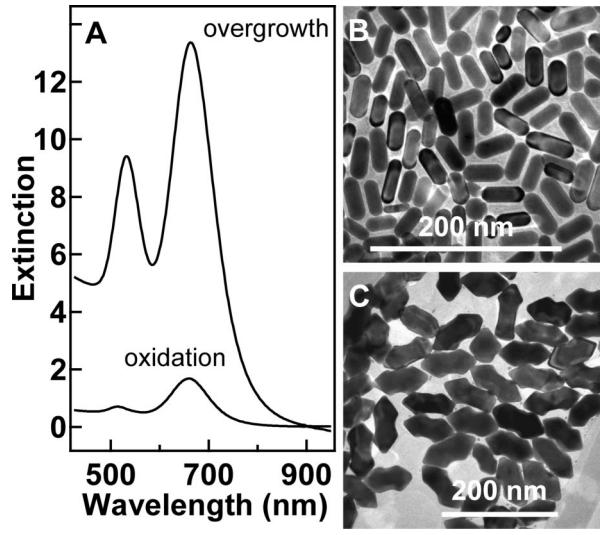

Figure 5. Comparison of two Au nanorod samples possessing similar LSPWs. (A) Extinction spectra of the two nanorod samples. The two extinction spectra have been scaled relative to the starting nanorod concentration. (B) and (C) TEM images of the Au nanorod samples obtained from shortening and overgrowth, respectively.

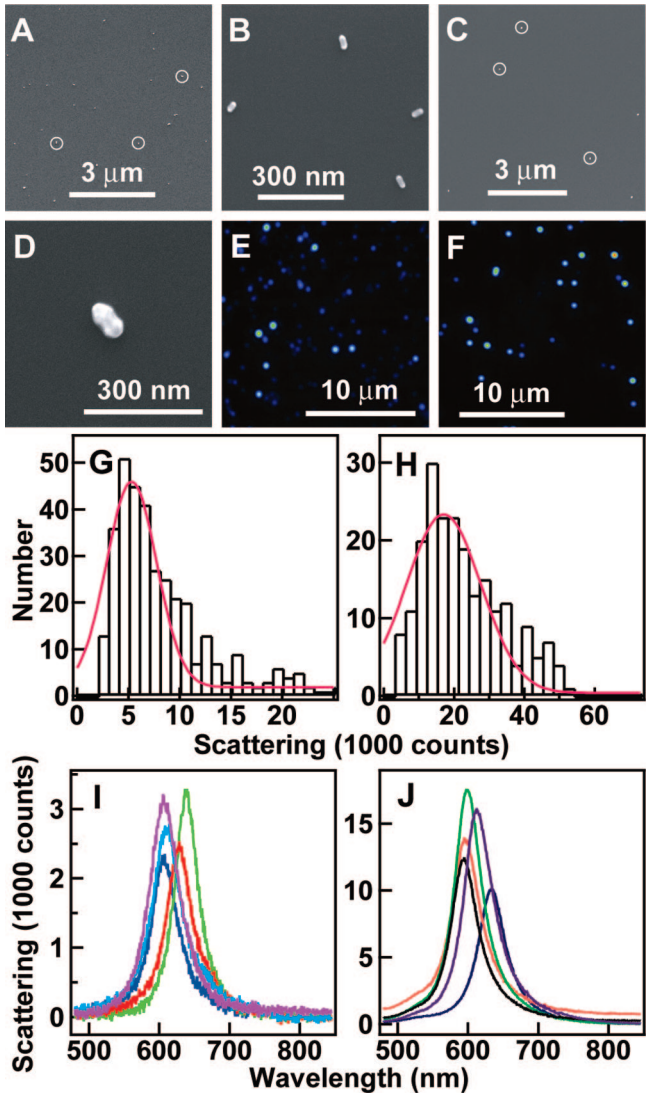

Figure 6. Single-particle dark-field imaging and spectroscopy. (A) and (B) Large-area and zoomed-in SEM images of the shortened Au nanorods. (C) and (D) Large-area and zoomed-in SEM images of the overgrown Au nanorods. Some nanorods are highlighted with circles in the large-area SEM images. (E) and (F) Dark-field images of the Au nanorods from shortening and overgrowth, respectively. The exposure times are 60 s for (E) and 5 s for (F). The color scales are the same for the two dark-field images. (G) and (H) Histograms of scattering intensities obtained from individual nanorods shown in (E) and (F), respectively. The red lines are Gaussian fits. (I) Five representative scattering spectra recorded for the nanorods shown in (E). The exposure time is 60 s. (J) Five representative scattering spectra recorded for the nanorods shown in (F). The exposure time is 10 s.

TABLE 1. Comparison of the Longitudinal Surface Plasmon Resonance-Related Properties between the Two Batches of Au Nanorod Samples

Au nanorod sample	from shortening	from overgrowth
diameter from TEM (nm)	17 ± 2	38 ± 4
length from TEM (nm)	40 ± 6	91 ± 8
ensemble LSPW (nm)	660	664
ensemble fwhm (nm/meV)	95/270	107/300
ensemble extinction[a]	1.69	13.37
dark-field LSPW (nm)	620 ± 12	600 ± 17
dark-field fwhm (nm/meV)	(49 ± 5)/(160 ± 20)	(52 ± 6)/(180 ± 30)
dark-field intensity (counts · s^{-1})[b]	89	3411
diameter for FDTD (nm)	16.5	38
length for FDTD (nm)	40	90
volume for FDTD (nm^3)	7377	73230
FDTD LSPW in solutions (nm)	656	661
FDTD fwhm in solutions (nm/meV) [c]	44/126	59/167
FDTD extinction in solutions (nm^2)[d]	5780	34400
FDTD scattering in solutions (nm^2)[e]	1570	16300
FDTD LSPW on glass (nm)	600	593
FDTD fwhm on glass (nm/meV) [f]	54/187	64/226
FDTD extinction on glass (nm^2)[d]	1787	21430
FDTD scattering on glass (nm^2)[e]	263	5430

[a]Peak values from Figure 5A. [b]Average scattering intensities determined from the Gaussian fits, as shown in Figure 6G and H. [c]For the extinction spectra. [d]Peak extinction cross sections. [e]Peak scattering cross sections. [f]For the scattering spectra.

semble extinction spectra acquired from the aqueous nanorod solutions. This blue-shift is due to that the refractive index of the surrounding medium for the nanorods deposited on glass slides is smaller than that for the nanorods dispersed in aqueous solutions. It has been known that a reduction in the index of the medium causes a blue-shift of the plasmon peak of noble metal nanoparticles.[41,42]

FDTD Calculation. Numerical calculations were performed to help understand our experimental results. Analytical solutions to Maxwell's equations have been derived previously for spherical[43] and prolate spheroidal particles.[35] In principle, the relative contributions of the scattering and absorption to the extinction of Au nanorods can be calculated according to these analytical solutions. However, a special code has to be developed to calculate the scattering and absorption properties of spheroidal particles. We instead chose FDTD for our purpose. The FDTD technique can provide a full range of plasmon resonance-related properties, [44] including extinction, scattering, absorption cross sections, and local electric fields, some of which are difficult to measure experimentally. The sizes of both Au nanorods were taken to match their average values. Specifically, the smaller nanorod is modeled as a cylinder capped with two half-spheres at the ends, with a diameter of 16.5 nm and a total length of 40 nm. The peanut-like larger nanorod is modeled as composed of a cylinder at the waist and a cone with four facetted surfaces at each end. The cylinder diameter is 38 nm, and the base diameter of the cone is 42 nm. The apex of the cone has an angle of 72.2°, and it is capped with a sphere of 7 nm diameter. The total length of the larger nanorod is 90 nm. For each nanorod, two types of surrounding environments were considered, corresponding to the cases of nanorods either dispersed in aqueous solutions or deposited on glass slides.

The calculated spectra for the two nanorod samples are shown in Figure 7, and some calculation results are listed in Table 1. First, the LSPWs of the nanorods deposited on glass slides are blue-shifted compared to those of the nanorods dispersed in aqueous solutions. Second, the extinction cross section (47% scattering + 53% absorption) of the larger nanorod is 6 times that

(27% scattering + 73% absorption) of the smaller nanorod in water, while the ratio of the extinction value between the larger and smaller nanorods measured from the ensemble solution samples is 8. Third, the scattering cross section (25% of extinction) of the larger nanorod is 21 times that (15% of extinction) of the smaller nanorod on glass slides, while the ratio of the scattering intensity between the larger and smaller nanorods measured from dark-field imaging is 38. Fourth, the FWHMs of the calculated scattering spectra for the nanorods sitting on glass slides are comparable to those determined from their dark-field scattering spectra. Taken together, the results from FDTD calculations are in very good agreement with those from experimental measurements. In addition, it is also noted that both the extinction cross sections and the scattering-to-extinction ratios of the nanorods deposited on glass slides are considerably smaller than those of the same nanorods dispersed in aqueous solutions. This dependence of the scattering and absorption properties of Au nanorods on their surrounding medium is worth further investigation because the use of Au nanorods for optical and biotechnological applications often requires that they are dispersed and incorporated into various materials, such as polymers, oxides, and biological molecules.

Our dark-field imaging experiments and FDTD calculations unambiguously demonstrate that the scattering-to-extinction ratio is dependent on the nanorod diameter even if the nanorod aspect ratio is fixed.To find out the changes of the longitudinal plasmon resonance-related properties as a function of the nanorod diameter while the nanorod aspect ratio is fixed, we further carried out FDTD calculations on Au nanorods that are dispersed in water and have aspect ratios fixed at 2.4 and diameters varying from 5 to 40 nm at a step of 5 nm. The chosen aspect ratio of 2.4 is equal to that of the Au nanorods characterized above using dark-field microscopy. Au nanorods with such a fixed aspect ratio and varying diameters can be produced by combining anisotropic shortening and transverse overgrowth and choosing appropriate starting nanorods.

Figure 8A shows the calculated maximum extinction, absorption, and scattering cross sections at the longitudinal plasmon peaks as a function of the nanorod diameter. They all increase nonlinearly as the nanorod diameter is increased. If the scattering-to-absorption (Figure 8B) and scattering-to-extinction (Figure 8C) ratios are plotted *versus* the nanorod diameter, it can be clearly seen that the absorption is dominant when the nanorod diameter is small, while the scattering becomes dominant when the nanorod diameter is large. Therefore, the relative contributions of the scattering and absorption to the extinction of Au nanorods with fixed aspect ratios can be experimentally controlled by varying their diameters. Such Au nanorods will be very useful for optical and biotechnological applications. For example, scattering-dominant nanorods

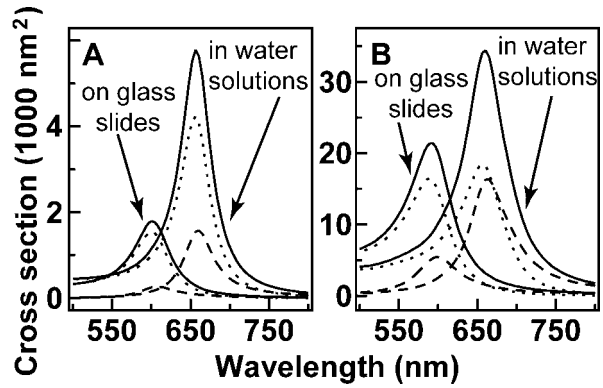

Figure 7. Extinction (solid lines), absorption (dotted lines), and scattering (dashed lines) spectra calculated using FDTD. (A) Calculated spectra of an averagely sized Au nanorod shown in Figure 5B. (B) Calculated spectra of an averagely sized Au nanorod shown in Figure 5C.

can minimize absorption-induced thermal damage during dark-field imaging and enhance sensitivity by maximizing the difference in the scattering-to-extinction ratio between contrast agents and tissues in optical coherence tomography,[45] while absorption-dominant nanorods can minimize the side effects caused by scattered light and reduce the laser energy required for photothermal treatment. Interestingly, the scattering-to-extinction ratio is seen to depend linearly on the nanorod diameter. A linear fitting gives a slope of 0.018 nm^{-1}. In addition, the LSPW is also seen to increase slightly as the diameter is increased (Figure 8D), even if the aspect ratio remains constant. This increase in the LSPW with increasing nanorod size at a fixed aspect ratio is different from what is predicted according to

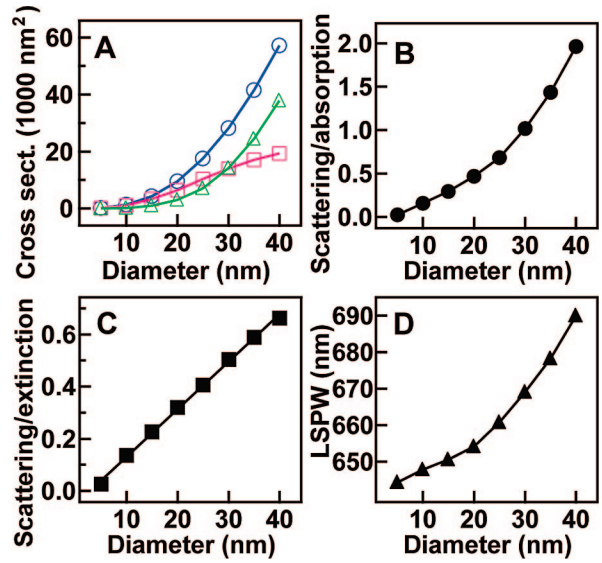

Figure 8. Effect of the nanorod diameter on the longitudinal plasmon resonance-related properties of Au nanorods investigated by FDTD calculations. (A) Extinction (circles), scattering (triangles), and absorption (squares) cross sections *versus* the diameter. (B) Ratio of the scattering to absorption cross section *versus* the diameter. (C) Ratio of the scattering to extinction cross section *versus* the diameter. The line is a linear fit. (D) LSPW *versus* the diameter. All the cross sections are peak values taken from corresponding calculated spectra.

Gans theory. The different results can be ascribed to that nanorods are treated as prolate spheroids in Gans theory without the consideration of phase retardation and higher-order contributions, while they are treated exactly according to their size and shape in FDTD calculations.

CONCLUSION

Anisotropic shortening and transverse overgrowth have been carried out to prepare Au nanorods of tunable LSPWs from the same starting nanorods. During shortening, the nanorod diameter remains nearly constant, while the nanorod length decreases gradually. Selective binding of thiol-containing molecules to the ends of Au nanorods induces overgrowth preferentially on their side surfaces. As a result, two series of Au nanorods with LSPWs varying from that of the starting nanorods to ~600 nm are obtained. The use of the same starting nanorods allows for a quantitative comparison of the extinction values between the two series of Au nanorods. The systematic variation of the LSPW and extinction is in good agreement with that obtained from Gans theory. Dark-field imaging and spectroscopy have been performed on two nanorod samples with one from shortening and the other from overgrowth. The two nanorod samples have similar LSPWs. It has been found that the scattering intensity of the overgrown nanorods is larger than that of the shortened nanorods. FDTD calculations have been carried out for the two nanorod samples. The experimental results are in very good agreement with the calculated ones, including the extinction values, scattering intensities, LSPWs, and FWHMs of the longitudinal plasmon peaks. FDTD calculations further show that the scattering-to-extinction ratio increases linearly as a function of the diameter for Au nanorods with a fixed aspect ratio. Absorption is dominant for nanorods with smaller diameters, while scattering becomes dominant for nanorods with large diameters. Such nanorods can potentially be produced by combining shortening and overgrowth and judiciously choosing starting nanorods with appropriate LSPWs. We believe that our results have great implications for the use of Au nanorods in a variety of optical and biotechnological applications.

METHODS

Growth of Starting Gold Nanorods. Starting Au nanorods were grown using the silver ion-assisted seed-mediated method.[25,26] Typically, the seed solution was prepared by the addition of $HAuCl_4$ (0.01 M, 0.25 mL) into cetyltrimethylammonium bromide (CTAB, 0.1 M, 10 mL) in a 15-mL plastic tube with gentle mixing. A freshly prepared, ice-cold $NaBH_4$ solution (0.01 M, 0.6 mL) was then injected quickly into the mixture solution, followed by rapid inversion for 2 min. The seed solution was kept at room temperature for at least 2 h before use. To grow Au nanorods, $HAuCl_4$ (0.01 M, 2.0 mL) and $AgNO_3$ (0.01 M, 0.4 mL) were mixed with CTAB (0.1 M, 40 mL) in a 50-mL plastic tube. HCl (1.0 M, 0.8 mL) was then added to adjust the pH of the solution to 1–2, followed by the addition of ascorbic acid (0.1 M, 0.32 mL). Finally, the seed solution (0.096 mL) was injected into the growth solution. The solution was gently mixed for 10 s and left undisturbed at room temperature for at least 6 h before use. Before the resulting Au nanorod solution was used for shortening and overgrowth, its pH was adjusted to 3–4 by the addition of NaOH (1.0 M, 0.8 mL).

Shortening of Gold Nanorods by Oxidation. The oxidation of Au nanorods was carried out by adding an appropriate volume of H_2O_2 (35 wt %) into the starting Au nanorod solution. The volume ratio of H_2O_2 to the starting nanorod solution was varied among 1:6, 1:8, 1:10, 1:50, and 1:60. The oxidation process was monitored by taking extinction spectra as a function of time. Shorter Au nanorods were obtained at intermediate stages of oxidation by centrifugation and redispersion of the resulting precipitates into water solutions.

Overgrowth on Gold Nanorods. A stock solution for overgrowth was prepared by mixing together CTAB (0.1 M, 152 mL), $HAuCl_4$ (0.01 M, 6.4 mL), $AgNO_3$ (0.01 M, 0.96 mL), and ascorbic acid (0.1 M, 1.024 mL). For overgrowth, 14 aliquots of 2 mL of the starting Au nanorod solution were placed into plastic tubes. Into the first 11 of them was added 0.03 mL of a cysteine solution (0.01 M), and into the other three was added 0.05 mL of the cysteine solution. After the resulting mixtures were kept at room temperature for 2 h, varying volumes of the stock growth solution (1, 2, 3, 4, 5, 7, 8, 10, 12, 15, 18, 20, 25, 30 mL, respectively) were added into each aliquot. The growth was left undisturbed for at least 10 h.

Extinction, SEM, and TEM Characterizations. Extinction spectra of Au nanorod solutions were taken using quartz cuvettes of 1-cm path length on a Hitachi U-3501 UV–visible/NIR spectrophotometer. SEM imaging was performed on a FEI Quanta 400 FEG microscope. Low-magnification TEM images were acquired on a FEI CM120 microscope at 120 kV. For TEM characterization, Au nanorod solutions (6 mL each) were centrifuged at 14 000*g* for 8 min. The precipitates were redispersed into deionized water (6 mL each), centrifuged again at 14 000*g* for 6 min, and finally redispersed into deionized water (0.4 mL each). An amount of 0.01 mL of each resulting Au nanorod solution was drop-cast carefully onto a lacey-Formvar TEM grid stabilized with a thin layer of carbon and allowed to dry in air overnight before TEM imaging.

Dark-Field Imaging of Individual Gold Nanorods. Au nanorods were deposited on silicon and glass substrates that were functionalized under the same conditions for SEM characterization and dark-field imaging, respectively. For functionalization, silicon and glass substrates were first washed in acetone, ethanol, and deionized water by ultrasonication and dried overnight at 60 °C. The cleaned substrates were then immersed in an ethanolic solution of (3-mercaptopropyl)trimethoxysilane (10 vol. %) for 15 min. The substrates were subsequently washed in ethanol by ultrasonication and finally rinsed with deionized water. For the deposition of Au nanorods onto the functionalized substrates, Au nanorod solutions (2 mL each) were centrifuged at 14 000*g* for 6 min, and the precipitates were redispersed in deionized water (2 mL each). This procedure was repeated once to remove excess CTAB present in Au nanorod solutions. The pH of each nanorod solution was adjusted to ~3 by adding HCl (0.1 M, 0.01 mL) to facilitate the deposition of Au nanorods. The functionalized substrates were then immersed into the resulting nanorod solutions for 30 s, rinsed immediately with ethanol, and blown dry with nitrogen. Dark-field imaging and spectroscopy on individual Au nanorods were carried out on an Olympus BX60 optical microscope integrated with an Acton SpectraPro 2300i monochromator and a Princeton Instruments Pixis 512B charge-coupled device (CCD), which was thermoelectrically cooled to −50 °C. Au nanorods deposited on glass slides were illuminated by white light from a 100 W tungsten lamp through an oil immersion dark-field condenser (NA 1.2–1.4). The scattered light was collected with a 100 × objective (NA 0.8) and reflected to

the entrance slit of the monochromator for imaging and spectroscopy. Scattering spectra from individual Au nanorods were corrected by subtracting background spectra taken from the adjacent regions containing no Au nanorods.

Modeling of the Longitudinal Surface Plasmon Resonance of Gold Nanorods with Gans Theory. Au nanorods were approximated as prolate spheroidal nanoparticles, and Gans theory[35] together with the known bulk Au dielectric function[36] was used to model the optical extinction spectra of Au nanorods of varying aspect ratios. According to Gans theory, the extinction cross section σ averaged over all orientations for a prolate spheroidal nanoparticle in the dipole approximation is given by

$$\sigma = \frac{2\pi V \varepsilon_m^{3/2}}{3\lambda} \sum_{j=1}^{3} \frac{(1/P_j^2)\varepsilon_2}{\left(\varepsilon_1 + \frac{1-P_j}{P_j}\varepsilon_m\right)^2 + \varepsilon_2^2} \quad (1)$$

In eq 1, V is the volume of the nanoparticle; ε_m is the dielectric constant of the surrounding medium; λ is the wavelength of the interacting light; ε_1 and ε_2 are the real and imaginary part of the Au dielectric function. ε_1 and ε_2 are wavelength dependent, while ε_m is assumed to be a constant. P_j (eqs 2 and 3) are the depolarization factors for the three axes A, B, and C of the spheroidal nanoparticle with $A > B = C$. They are defined as

$$P_A = \frac{1-e^2}{e^2}\left[\frac{1}{2e}\ln\left(\frac{1+e}{1-e}\right) - 1\right] \quad (2)$$

$$P_B = P_C = \frac{1-P_A}{2} \quad (3)$$

In eq 2, e is defined by

$$e = \sqrt{1 - \left(\frac{B}{A}\right)^2} \quad (4)$$

The ratio A/B in eq 4 is the aspect ratio. The volume (eq 5) of the spheroidal nanoparticle is given by

$$V = \frac{4\pi}{3}\left(\frac{A}{2}\right)\left(\frac{B}{2}\right)\left(\frac{C}{2}\right) \quad (5)$$

In our modeling, the medium dielectric constant was taken to be 2.0, which has previously been shown to be appropriate for modeling the extinction spectra of CTAB-stabilized Au nanorods in aqueous solutions.[37]

FDTD Calculations. The FDTD method is an explicit time marching algorithm used to solve Maxwell's curl equations on a discretized spatial grid. It can be used to study both the near- and far-field electromagnetic responses of metal nanoparticles of arbitrary shapes. We employed a software package, FDTD Solutions, developed by Lumerical Solutions, Inc., to perform FDTD calculations on Au nanorods. The Au dielectric function was represented using the Drude model,[44] with parameters chosen to match the bulk gold dielectric data.[36] In our FDTD calculations, a nanorod was surrounded by a virtual boundary with an appropriate size. The Au nanorod and its surrounding medium inside the boundary were divided into meshes of 0.5 nm in size. An electromagnetic pulse was launched into the boundary to simulate a propagating plane wave interacting with the nanorod. Only the longitudinal plasmon resonance of Au nanorods was calculated by setting the electric field of the plane wave parallel to the length direction of Au nanorods. FDTD calculations were carried out for both Au nanorods dispersed in aqueous solutions and those deposited on glass substrates to compare the calculation results with the experimental ones obtained from extinction measurements and dark-field spectroscopy, respectively. For Au nanorods dispersed in aqueous solutions, the refractive index of the surrounding medium was taken to be 1.33. For Au nanorods deposited on glass substrates, the refractive index of the medium in the top and side regions was taken to be 1.0, and that in the bottom region was taken to be 1.514.

Acknowledgment. Support from the RGC Research Grant Direct Allocation (Project Code: 2060306) and a RGC CERG grant (ref. No.: 403006, Project Code: 2160293) is gratefully acknowledged. The authors are grateful for the help in FDTD calculations from Lumerical Solutions, Inc. and the CUHK High Performance Computing support team.

Supporting Information Available: TEM image and extinction spectrum of the starting Au nanorods. This material is available free of charge via the Internet at http://pubs.acs.org.

REFERENCES AND NOTES

1. Lee, K.-S.; El-Sayed, M. A. Dependence of the Enhanced Optical Scattering Efficiency Relative to That of Absorption for Gold Metal Nanorods on Aspect Ratio, Size, End-Cap Shape, and Medium Refractive Index. *J. Phys. Chem. B* **2005**, *109*, 20331–20338.
2. Jain, P. K.; Lee, K. S.; El-Sayed, I. H.; El-Sayed, M. A. Calculated Absorption and Scattering Properties of Gold Nanoparticles of Different Size, Shape, and Composition: Applications in Biological Imaging and Biomedicine. *J. Phys. Chem. B* **2006**, *110*, 7238–7248.
3. Chen, W. R.; Adams, R. L.; Carubelli, R.; Nordquist, R. E. Laser-Photosensitizer Assisted Immunotherapy: A Novel Modality for Cancer Treatment. *Cancer Lett.* **1997**, *115*, 25–30.
4. Gorelikov, I.; Field, L. M.; Kumacheva, E. Hybrid Microgels Photoresponsive in the Near-Infrared Spectral Range. *J. Am. Chem. Soc.* **2004**, *126*, 15938–15939.
5. Karg, M.; Pastoriza-Santos, I.; Pérez-Juste, J.; Hellweg, T.; Liz-Marzán, L. M. Nanorod-Coated PNIPAM Microgels: Thermoresponsive Optical Properties. *Small* **2007**, *3*, 1222–1229.
6. Pérez-Juste, J.; Rodríguez-González, B.; Mulvaney, P.; Liz-Marzán, L. M. Optical Control and Patterning of Gold-Nanorod-Poly(vinyl alcohol) Nanocomposite Films. *Adv. Funct. Mater.* **2005**, *15*, 1065–1071.
7. Murphy, C. J.; Orendorff, C. J. Alignment of Gold Nanorods in Polymer Composites and on Polymer Surfaces. *Adv. Mater.* **2005**, *17*, 2173–2177.
8. Chon, J. W. M.; Bullen, C.; Zijlstra, P.; Gu, M. Spectral Encoding on Gold Nanorods Doped in a Silica Sol-Gel Matrix and Its Application to High-Density Optical Data Storage. *Adv. Funct. Mater.* **2007**, *17*, 875–880.
9. Berry, V.; Gole, A.; Kundu, S.; Murphy, C. J.; Saraf, R. F. Deposition of CTAB-Terminated Nanorods on Bacteria to Form Highly Conducting Hybrid Systems. *J. Am. Chem. Soc.* **2005**, *127*, 17600–17601.
10. Katz, E.; Willner, I. Integrated Nanoparticle-Biomolecule Hybrid Systems: Synthesis, Properties, and Applications. *Angew. Chem., Int. Ed.* **2004**, *43*, 6042–6108.
11. Sudeep, P. K.; Joseph, S. T. S.; Thomas, K. G. Selective Detection of Cysteine and Glutathione Using Gold Nanorods. *J. Am. Chem. Soc.* **2005**, *127*, 6516–6517.
12. Wang, H. F.; Huff, T. B.; Zweifel, D. A.; He, W.; Low, P. S.; Wei, A.; Cheng, J.-X. *In Vitro* and *In Vivo* Two-Photon Luminescence Imaging of Single Gold Nanorods. *Proc. Natl. Acad. Sci. U.S.A.* **2005**, *102*, 15752–15756.
13. Durr, N. J.; Larson, T.; Smith, D. K.; Korgel, B. A.; Sokolov, K.; Ben-Yakar, A. Two-Photon Luminescence Imaging of Cancer Cells Using Molecularly Targeted Gold Nanorods. *Nano Lett.* **2007**, *7*, 941–945.
14. Huang, X. H.; El-Sayed, I. H.; Qian, W.; El-Sayed, M. A. Cancer Cells Assemble and Align Gold Nanorods Conjugated to Antibodies to Produce Highly Enhanced, Sharp, and Polarized Surface Raman Spectra: A Potential Cancer Diagnostic Marker. *Nano Lett.* **2007**, *7*, 1591–1597.
15. Huang, X. H.; El-Sayed, I. H.; Qian, W.; El-Sayed, M. A. Cancer Cell Imaging and Photothermal Therapy in the Near-Infrared Region by Using Gold Nanorods. *J. Am. Chem. Soc.* **2006**, *128*, 2115–2120.
16. Chen, C.-C.; Lin, Y.-P.; Wang, C.-W.; Tzeng, H.-C.; Wu, C.-H.; Chen, Y.-C.; Chen, C.-P.; Chen, L.-C.; Wu, Y.-C. DNA-Gold Nanorod Conjugates for Remote Control of Localized

Gene Expression by Near Infrared Irradiation. *J. Am. Chem. Soc.* **2006**, *128*, 3709–3715.
17. Weissleder, R. A Clearer Vision for *In Vivo* Imaging. *Nat. Biotechnol.* **2001**, *19*, 316–317.
18. Hirsch, L. R.; Stafford, R. J.; Bankson, J. A.; Sershen, S. R.; Rivera, B.; Price, R. E.; Hazle, J. D.; Halas, N. J.; West, J. L. Nanoshell-Mediated Near-Infrared Thermal Therapy of Tumors under Magnetic Resonance Guidance. *Proc. Natl. Acad. Sci. U.S.A.* **2003**, *100*, 13549–13554.
19. Loo, C.; Lowery, A.; Halas, N.; West, J.; Drezek, R. Immunotargeted Nanoshells for Integrated Cancer Imaging and Therapy. *Nano Lett.* **2005**, *5*, 709–711.
20. Chen, J. Y.; Saeki, F.; Wiley, B. J.; Cang, H.; Cobb, M. J.; Li, Z.-Y.; Au, L.; Zhang, H.; Kimmey, M. B.; Li, X. D.; Xia, Y. N. Gold Nanocages: Bioconjugation and Their Potential Use as Optical Imaging Contrast Agents. *Nano Lett.* **2005**, *5*, 473–477.
21. Jana, N. R.; Gearheart, L.; Murphy, C. J. Wet Chemical Synthesis of High Aspect Ratio Cylindrical Gold Nanorods. *J. Phys. Chem. B* **2001**, *105*, 4065–4067.
22. Kim, F.; Song, J. H.; Yang, P. D. Photochemical Synthesis of Gold Nanorods. *J. Am. Chem. Soc.* **2002**, *124*, 14316–14317.
23. Busbee, B. D.; Obare, S. O.; Murphy, C. J. An Improved Synthesis of High-Aspect-Ratio Gold Nanorods. *Adv. Mater.* **2003**, *15*, 414–416.
24. Pérez-Juste, J.; Liz-Marzán, L. M.; Carnie, S.; Chan, D. Y. C.; Mulvaney, P. Electric-Field-Directed Growth of Gold Nanorods in Aqueous Surfactant Solutions. *Adv. Funct. Mater.* **2004**, *14*, 571–579.
25. Nikoobakht, B.; El-Sayed, M. A. Preparation and Growth Mechanism of Gold Nanorods (NRs) Using Seed-Mediated Growth Method. *Chem. Mater.* **2003**, *15*, 1957–1962.
26. Sau, T. K.; Murphy, C. J. Seeded High Yield Synthesis of Short Au Nanorods in Aqueous Solution. *Langmuir* **2004**, *20*, 6414–6420.
27. Kou, X. S.; Zhang, S. Z.; Tsung, C.-K.; Yeung, M. H.; Shi, Q. H.; Stucky, G. D.; Sun, L. D.; Wang, J. F.; Yan, C. H. Growth of Gold Nanorods and Bipyramids Using CTEAB Surfactant. *J. Phys. Chem. B* **2006**, *110*, 16377–16383.
28. Kou, X. S.; Zhang, S. Z.; Tsung, C.-K.; Yang, Z.; Yeung, M. H.; Stucky, G. D.; Sun, L. D.; Wang, J. F.; Yan, C. H. One-Step Synthesis of Large-Aspect-Ratio Single-Crystalline Gold Nanorods by Using CTPAB and CTBAB Surfactants. *Chem.—Eur. J.* **2007**, *13*, 2929–2936.
29. Tsung, C.-K.; Kou, X. S.; Shi, Q. H.; Zhang, J. P.; Yeung, M. H.; Wang, J. F.; Stucky, G. D. Selective Shortening of Single-Crystalline Gold Nanorods by Mild Oxidation. *J. Am. Chem. Soc.* **2006**, *128*, 5352–5353.
30. Kou, X. S.; Zhang, S. Z.; Yang, Z.; Tsung, C.-K.; Stucky, G. D.; Sun, L. D.; Wang, J. F.; Yan, C. H. Glutathione- and Cysteine-Induced Transverse Overgrowth on Gold Nanorods. *J. Am. Chem. Soc.* **2007**, *129*, 6402–6404.
31. Zweifel, D. A.; Wei, A. Sulfide-Arrested Growth of Gold Nanorods. *Chem. Mater.* **2005**, *17*, 4256–4261.
32. Zhang, S. Z.; Kou, X. S.; Yang, Z.; Shi, Q. H.; Stucky, G. D.; Sun, L. D.; Wang, J. F.; Yan, C. H. Nanonecklaces Assembled from Gold Rods, Spheres, and Bipyramids. *Chem. Commun.* **2007**, 1816–1818.
33. Liao, H. W.; Hafner, J. H. Gold Nanorod Bioconjugates. *Chem. Mater.* **2005**, *17*, 4636–4641.
34. Orendorff, C. J.; Murphy, C. J. Quantitation of Metal Content in the Silver-Assisted Growth of Gold Nanorods. *J. Phys. Chem. B* **2006**, *110*, 3990–3994.
35. Gans, R. Form of Ultramicroscopic Particles of Silver. *Ann. Phys. (Leipzig)* **1915**, *47*, 270–284.
36. Johnson, P. B.; Christy, R. W. Optical Constants of the Noble Metals. *Phys. Rev. B* **1972**, *6*, 4370–4379.
37. Link, S.; Mohamed, M. B.; El-Sayed, M. A. Simulation of the Optical Absorption Spectra of Gold Nanorods as a Function of Their Aspect Ratio and the Effect of the Medium Dielectric Constant. *J. Phys. Chem. B* **1999**, *103*, 3073–3077.
38. Gulati, A.; Liao, H. W.; Hafner, J. H. Monitoring Gold Nanorod Synthesis by Localized Surface Plasmon Resonance. *J. Phys. Chem. B* **2006**, *110*, 22323–22327.
39. Sönnichsen, C.; Franzl, T.; Wilk, T.; von Plessen, G.; Feldmann, J. Drastic Reduction of Plasmon Damping in Gold Nanorods. *Phys. Rev. Lett.* **2002**, *88*, 077402.
40. Sönnichsen, C.; Alivisatos, A. P. Gold Nanorods as Novel Nonbleaching Plasmon-Based Orientation Sensors for Polarized Single-Particle Microscopy. *Nano Lett.* **2005**, *5*, 301–304.
41. Mock, J. J.; Smith, D. R.; Schultz, S. Local Refractive Index Dependence of Plasmon Resonance Spectra from Individual Nanoparticles. *Nano Lett.* **2003**, *3*, 485–491.
42. McFarland, A. D.; Van Duyne, R. P. Single Silver Nanoparticles as Real-Time Optical Sensors with Zeptomole Sensitivity. *Nano Lett.* **2003**, *3*, 1057–1062.
43. Mie, G. A Contribution to the Optics of Turbid Media Special Colloidal Metal Solutions. *Ann. Phys. (Leipzig)* **1908**, *25*, 377–445.
44. Oubre, C.; Nordlander, P. Optical Properties of Metallodielectric Nanostructures Calculated Using the Finite Difference Time Domain Method. *J. Phys. Chem. B* **2004**, *108*, 17740–17747.
45. Oldenburg, A. L.; Hansen, M. N.; Zweifel, D. A.; Wei, A.; Boppart, S. A. Plasmon-Resonant Gold Nanorods as Low Backscattering Albedo Contrast Agents for Optical Coherence Tomography. *Opt. Express* **2006**, *14*, 6724–6738.